A Discontinuous Galerkin Method for the Hall MHD Equations (PREPRINT)*

J. Loverich†

Tech-X Corporation

J-L. Cambier

AFRL Edwards

In this paper a discontinuous Galerkin method for the Hall MHD equations is developed. Simulations are performed with 2^{nd}, 3^{rd} and 4^{th} order schemes using either component or characteristic based limiters. The equations are formulated in gas dynamic conservative form and tested on the Brio and Wu MHD shock as well as the GEM challenge magnetic reconnection problem. Solutions compare well with previously published results. The algorithm is easily extended to general geometries.

I. INTRODUCTION

In fluid plasma physics ideal MHD (Magnetohydrodynamics) is identified by the ideal Ohm's law $E = -U \times B$ where E, U, B are the electric field, bulk fluid velocity and magnetic field respectively. This version of Ohm's law is derived under the assumption that the ions are well magnetized. This assumption breaks down on the scale of the ion inertial length or the ion Larmor radius and additional terms must be kept during the derivation, the addition of the Hall term describes large Larmor radius effects where the magnetic field is no longer frozen to the ions, but instead is frozen to the electrons. Ohm's law then becomes $E = u_e \times B$ where u_e is the electron fluid velocity. For many plasma devices it is important to model ion demagnetization including FRCs (field reversed configurations) Z-Pinches when the pinch radius is on the order of a few ion Larmor radii and any other device where the ion inertial length is on the same scale as the plasma. Furthermore, a number of instabilities arise in part due to the Hall term which can lead to anomalous resistivity in current layers. The goal of this paper is to present an algorithm using the discontinuous Galerkin (DG) method which can be used to model high beta plasmas where ion demagnetization effects are important. Furthermore, the scheme is a shock capturing scheme since we are interested in potentially violent behaviors in plasmas such as FRC formation, non-collisional reconnection and fast instabilities.

Hall MHD has been studied by many authors and several algorithms have been developed, the papers by (4; 12; 14; 15) give a few example of Hall MHD algorithms though many others have been published. The discontinuous Galerkin technique is an traditionally explicit finite element technique that is currently very popular in the hyperbolic algorithms community. The technique is designed for general geometry and arbitrary order accuracy. For linear systems the technique works as advertised and spectral order accuracy can be achieved under *hp* refinement. The goal of application of the discontinuous Galerkin technique to non-linear systems is to achieve the same sorts of benefits and ultimately produce better solutions at reduced computational cost. The technique has achieved varrying degrees of success when applied to non-linear problems. The authors have found that the discontinuous Galerkin approach has additional benefits compared to simpler techniques such as finite volumes when solutions are in quasi-equilibrium where fluxes are balancing source terms. For example when simulating a Z-pinch instability finite volume techniques tend to smear out the initial equilibrium more than discontinuous Galerkin techniques(26) even for the same order accuracy - this is only an issue when your algorithm cannot be written in conservative form or is not written in conservative form. This implies that even a second order discontinuous Galerkin algorithm may have advantages over other existing second order methods(26) such as second order finite volume schemes.

The discontinuous Galerkin technique has been applied to many plasma systems (18; 21; 28) and the technique is discussed in great detail in general terms in the textbook by Hesthaven and Warburton (13). In the current work the discontinuous Galerkin method is used and the algorithm is developed from the Hall MHD equations in gas dynamic form similar to the approach taken in solving the two-fluid equations in (25).

---

*Distribution A: Public Release, Distribution Unlimited

†Electronic address: loverich@txcorp.com; formerly an employee of Advatech Pacific

II. SYSTEM OF EQUATIONS

The model is derived by assuming that the speed of light is large in comparison to other speeds in the system and that electron inertia is negligible. Furthermore, quasi-neutrality is assumed, so that only one continuity equation is required,

$$\frac{\partial \rho_i}{\partial t} + \nabla \cdot [\rho_i \, U_i] = 0 \,, \tag{1}$$

A momentum equation for the ions is used,

$$\frac{\partial \rho_i \, U_i}{\partial t} + \nabla \cdot [\rho_i \, U_i \, U_i + P_i] = n_i \, q_i \, E + J_i \times B \,, \tag{2}$$

as well as an ion energy equation,

$$\frac{\partial e_i}{\partial t} + \nabla \cdot [U_i \, (e_i + P_i)] = J_i \cdot E \,, \tag{3}$$

where e_i is the ion kinetic energy + internal energy, and an electron energy equation,

$$\frac{\partial e_e}{\partial t} + \nabla \cdot [U_e \, (e_e + P_e)] = J_e \cdot E \,. \tag{4}$$

where e_e is the electron kinetic energy + the electron internal energy - however, electron kinetic energy is zero because the electron mass is set to zero. The species currents are J_α where $\alpha = e, i$ for the electrons and ions respectively. The ideal gas equation of state is used, therefore $P_i = n_i \, k \, T_i$ and $P_e = n_e \, k \, T_e$. The completeness of the system requires a momentum equation for the electron fluid. Since the electrons are assumed massless the convective derivative is set to zero and we are left with pressure and Lorentz forces. In this paper we only focus on the non-dissipative ideal terms, so resistivity is ignored. The reduced electron momentum equation or Ohm's law, is given by

$$\Psi = n_e \, q_e \, E = -J_e \times B + \nabla \, P_e \,. \tag{5}$$

The magnetic field equation is also included

$$\frac{\partial B}{\partial t} + \nabla \times E = 0 \,. \tag{6}$$

In this paper errors in $\nabla \cdot B$ are kept small by using the hyperbolic divergence cleaning method as suggested in (10). Using this formulation an additional equation is added and the magnetic field equation is modified, thus

$$\frac{\partial B}{\partial t} + \nabla \times E + \nabla \phi = 0 \,. \tag{7}$$

and

$$\frac{\partial \phi}{\partial t} + \Gamma^2 \nabla \cdot B = -\zeta \phi \,. \tag{8}$$

The modified magnetic field equation adds the divergence wave to the system which propagates divergence errors out of the domain at speed Γ while simultaneously damping them. This wave is small in magnitude because the divergence errors are small and contributes very little to the magnetic field. A linear wave analysis shows that this divergence wave does not modify other linear plasma waves in 1D.

III. DISPERSION RELATION

The whistler wave in Hall MHD has a dispersion relation solutions where the frequency ω is quadratic in the wave number k. This differs from ideal MHD where all dispersion relations are proportional to k. This fact is important because it means that in Hall MHD when the whistler wave dominates the time step Δt is proportional to Δx^2.

We briefly consider only the dispersion relation when the wave propagates parallel to the magnetic field.

$$\omega = \frac{B_0}{2q\,n_0\,\mu_0}k^2 + \frac{B_0\sqrt{4\,n_0\,m_i\,\mu_0\,q^2 + k^2\,m_i^2}}{2\,q\,m_i\,n_0\,\mu_0}\,k\,. \tag{9}$$

Note that this can be written

$$\omega = \frac{1}{2}\omega_{c\,i}\,d_i^2\,k^2 + \sqrt{V_A^2k^2 + \frac{1}{2}\,\omega_{c\,i}^2\,d_i^4\,k^4}\,, \tag{10}$$

where $d_i = \frac{c}{\omega_{p\,i}} = c\sqrt{\frac{m_i\,\epsilon_0}{n_0\,q^2}}$ is the ion inertial length or ion skin depth, $V_A = \frac{B_0}{\sqrt{n_0 m_i\,\mu_0}}$ is the Alfven wave speed. The whistler wave becomes,

$$\omega = \omega_{c\,i}\,d_i^2\,k^2 \tag{11}$$

for sufficiently large k. The importance of the Hall term (and hence the whistler wave) can be determined by the ratio of the contributions of the quadratic and linear terms in the whistler wave dispersion relation, thus, the whistler wave is important when,

$$\frac{V_w}{V_A}k = d_i k \gtrapprox 1\,, \tag{12}$$

where $V_w = \omega_{c\,i}d_i^2 = \frac{B_0}{q\,n_0\,\mu_0}$. This condition implies that the Hall term is important for frequencies where $\omega \gtrapprox \omega_{c\,i}$ and for wavelengths $L = \frac{2\pi}{k}$ where $L \lessapprox d_i$.

For small wave numbers this dispersion relation results in an Alfven wave dispersion relation and ω varies linearly with k as in ideal MHD. In the limit of large wave numbers ω varies quadratically with k. In general, we have traditional convection combined with dispersive convection. This sort of consideration suggests the following system as a simple model for the ideal Hall MHD system

$$\frac{\partial u}{\partial t} = \delta_1\frac{\partial u}{\partial x} - i\,\delta_2\frac{\partial^2 u}{\partial x^2}\,. \tag{13}$$

If the non-dispersive advective term is ignored we simply have,

$$\frac{\partial u}{\partial t} = -i\,\delta_2\frac{\partial^2 u}{\partial x^2}\,. \tag{14}$$

which is equivalent to the Schrodinger equation. Fortunately, numerical solutions to the Schrodinger equation have been studied for decades, see for example (5), and basic stable schemes can be borrowed from previous work on the Schrodinger system in addition to the Hall MHD system.

In an explicit code the previous analysis suggests the following time step restrictions. First of all the magnetosonic wave V_m should be resolved, thus

$$\Delta t < \frac{\Delta x}{|U| + V_m} \tag{15}$$

From the parallel whistler wave dispersion relation the maximum time step should be

$$\Delta t < \frac{\Delta x^2}{V_w} \tag{16}$$

when the whistler term dominates. In general then,

$$\Delta t < \min\left[\frac{\Delta x}{|U| + V_m}, \frac{\Delta x^2}{V_w}\right] \tag{17}$$

Drift waves also exist in the Hall MHD system and the actual time step may be more restrictive. Huba discusses this in more detail in (15). For many problems the Whistler wave dominates and taking a time step based on its value is frequently adequate.

IV. NUMERICAL APPROACH

The numerical approach used is the discontinuous Galerkin method. The discontinuous Galerkin method can be considered an extension of finite volume methods or a finite element method where the solution can be discontinuous at nodes. The technique is described for hyperbolic systems in (6–9). The recent book by Hesthaven and Warburton (13) describes the DG methods in detail and should be used when generalizing the algorithm to unstructured meshes or to provide further incite into the technique. The method is explicit and does not require the solution of a global mass matrix at each time step so the scheme is highly parallelizable.

A. Scalar example

We begin the derivation by applying the numerical approach to the simple model problem (13) before going into the full system. First re-write (13) as a system of equations using $f = -\left(\delta_1 u - i\delta_2 v\right)$.

$$\frac{\partial u}{\partial t} = -\frac{\partial f}{\partial x} \tag{18}$$

$$v = \frac{\partial u}{\partial x}\,. \tag{19}$$

In these equations u is called a balance variable and v is an auxiliary variable. The first task is to project the equations onto a set of basis function, in this case Legendre polynomials. The r^{th} Legendre polynomial is denoted h_r. The projection is first performed on the auxiliary equation (19). Multiplying by h_r and integrating gives

$$\int_{x_{i-1/2}}^{x_{i+1/2}} v\, h_r\, dx = \int_{x_{i-1/2}}^{x_{i+1/2}} \frac{\partial u}{\partial x}\, h_r\, dx. \tag{20}$$

integrating the right hand side by parts produces

$$\int_{x_{i-1/2}}^{x_{i+1/2}} v\, h_r\, dx = \left(u_{i+1/2}\, h_{r\,i+1/2} - u_{i-1/2}\, h_{r\,i-1/2}\right) - \int_{x_{i-1/2}}^{x_{i+1/2}} u\, \frac{\partial h_r}{\partial x}\, dx. \tag{21}$$

The first term on the right hand side of 21 is considered the flux term and is responsible for exchanging data between cells. The value of $u\, h_r$ is undefined at the cell edge since in general it has two values at that location, one value from the left cell and one value from the right cell. The choice of flux function will be discussed later.

Within each computational cell u and v are approximated as a sum of the basis functions,

$$\tilde{u} = \sum_s u_s\, h_s \tag{22}$$

$$\tilde{v} = \sum_s v_s\, h_s\,. \tag{23}$$

Substituting these into the remaining integral terms in 21 and dropping the integral ranges gives

$$\sum_s v_s \int h_s\, h_r\, dx = \left(u_{i+1/2}\, h_{r\,i+1/2} - u_{i-1/2}\, h_{r\,i-1/2}\right) - \sum_s u_s \int h_s\, \frac{\partial h_r}{\partial x}\, dx. \tag{24}$$

Letting $H_{s\,r} = \int h_s\, h_r\, dx$ equation (24) can be written as a matrix vector equation so that

$$v_s = H^{-1}_{s\,r}\, \mathrm{Ra}_r\,. \tag{25}$$

where

$$\mathrm{Ra}_r = \left(u_{i+1/2}\, h_{r\,i+1/2} - u_{i-1/2}\, h_{r\,i-1/2}\right) - \sum_s u_s \int h_s\, \frac{\partial h_r}{\partial x}\, dx \tag{26}$$

An identical expansion for the balanced variables results in

$$\frac{\partial u_s}{\partial t} = H^{-1}_{s\,r}\,\mathrm{Rc}_r\,. \tag{27}$$

where

$$\mathrm{Rc}_r = -\left(f_{i+1/2}\,h_{r\,i+1/2} - f_{i-1/2}\,h_{r\,i-1/2}\right) + \sum_s f\left(u_s, v_s\right)\int h_s\,\frac{\partial h_r}{\partial x}\,dx\,. \tag{28}$$

When h_r are orthogonal and regular geometry is used $H_{s\,r}$ is diagonal. The only structural difference between equation (25) and (27) is the presence of a time derivative on the left hand side of equation (27). The time derivative can be evaluated using a Runge-Kutta method, we typically use 3^{rd} or 4^{th} order Runge-Kutta method. The auxiliary variables are updated before each substep of the Runge-Kutta method.

B. Hall MHD case

Start by defining n auxiliary variables. In the case of Hall MHD with diamagnetic drift, n is 2. These auxiliary variables are written generically as,

$$v_1 = \nabla\cdot w_1\left(q, v_1\right) + \psi_1\left(q, v_1, \mathbf{r}\right)\,. \tag{29}$$

$$v_2 = \nabla\cdot w_2\left(q, v_2, v_1\right) + \psi_2\left(q, v_2, v_1, \mathbf{r}\right)\,. \tag{30}$$

and finally,

$$v_n = \nabla\cdot w_n\left(q, v_{n-1}, ..., v_1\right) + \psi_n\left(q, v_{n-1}, ..., v_1, \mathbf{r}\right)\,. \tag{31}$$

The q are balance variables, the v are auxiliary variables, the w are flux functions and the ψ are terms that only depend on algebraic combinations of q, v, and $\mathbf{r}$ where $\mathbf{r}$ is a vector position. Using the above formulation the Hall MHD system can be described. The auxiliary variables for the Hall MHD system are defined as,

$$v_1 = J = \frac{1}{\mu_0}\nabla\times B \tag{32}$$

and

$$v_2 = \Psi = n_e\,q_e\,E = -\left(J - J_i\right)\times B + \nabla\,P_e\,. \tag{33}$$

In addition, take the balance law,

$$\frac{\partial\,q}{\partial\,t} + \nabla\cdot f\left(q, v_n, ..., v_2, v_1\right) = \psi\left(q, v_n, ..., v_2, v_1, \mathbf{r}\right) \tag{34}$$

where f is a flux function.

The balance law represents each of the equations with time derivatives in them in the Hall MHD system. The approach is to solve for the auxiliary variables one after another, using the solution v_{n-1} to solve for v_n, then substitute these solution into the balance law.

Using quadrilateral elements, Legendre polynomials are used as basis function and each of the variables v_n and q_n are represented as a linear combination of Legendre polynomials. Therefore if the basis set is h_r, where h_r is the rth Legendre polynomial, then the variables are represented as,

$$\tilde{v}_n = \sum_{r=0}^{p-1}\alpha_{n\,r}h_r\,, \tag{35}$$

$$\tilde{q}_n = \sum_{r=0}^{p-1}\beta_{n\,r}h_r\,, \tag{36}$$

where p is the number of basis functions in the expansion. In 1-D, p corresponds to the order of accuracy of the scheme. In 2-D for a strictly n^{th} order scheme $p = \frac{1}{2}(n+1)\, n$ where 2D Legendre polynomials are used as the bases. In equation (35) $\alpha_{n\,r}$ represents the r^{th} basis coefficient of the n^{th} auxiliary variable and in equation (36) $\beta_{n\,r}$ represents the r^{th} coefficient of the n^{th} balance variable. For a system of one auxiliary variable and one balance variable you can eliminate the subscript n to arrive at a system like that discussed in the previous section. These same basis functions are used to expand the system of equations. First the auxiliary variables are considered. Multiply the equation (31) by the basis function set h_r and integrate over the volume to get,

$$\int_\Omega \tilde{v}_n\, h_r\, d\Omega = \int_\Omega \nabla \cdot w_n\left(q, \tilde{v}_{n-1}, ..., \tilde{v}_1\right)\, h_r\, d\Omega + \int_\Omega \psi_n\left(\tilde{q}, \tilde{v}_{n-1}, ..., \tilde{v}_1, \mathbf{r}\right)\, h_r\, d\Omega \tag{37}$$

Integration by parts is applied to the derivative to yield,

$$\int_\Omega \tilde{v}_n\, h_r\, d\Omega = \int_{\partial\Omega} \left[w_n\left(\tilde{q}, \tilde{v}_{n-1}, ..., \tilde{v}_1\right)\, h_r\right] \cdot \bar{n}\, d\partial\Omega - \int_\Omega w_n\left(\tilde{q}, \tilde{v}_{n-1}, ..., \tilde{v}_1\right) \cdot \nabla\, h_r\, d\Omega + \int_\Omega \psi_n\left(\tilde{q}, \tilde{v}_{n-1}, ..., \tilde{v}_1, \mathbf{r}\right)\, h_r\, d\Omega = T_{n\,r} \tag{38}$$

Substituting the definition of $\tilde{v}_n$ (35) into the first term of equation (38), the following result is obtained

$$\int_\Omega \tilde{v}_n\, h_r\, d\Omega = \sum_{g=0}^{p-1} \alpha_{n\,g} \int_\Omega h_g\, h_r\, d\Omega = \sum_{g=0}^{p-1} \alpha_{n\,g}\, H_{g\,r} \tag{39}$$

so that

$$H_{g\,r} = \int_\Omega h_g\, h_r\, d\Omega\,. \tag{40}$$

On a regular cartesian grid, $H_{g\,r}$ is diagonal since the basis functions are orthogonal. Now the coefficients $\alpha_{n\,g}$ can be calculated based on a numerical solution to the right hand side of (38), so that if we assume $M_{g\,r} = H^{-1}_{g\,r}$, then

$$\alpha_{n\,g} = T_{n\,r} M_{g\,r} \tag{41}$$

where summation on the repeated index r is assumed. $M_{g\,r}$ is a square matrix of size $p \times p$, $\alpha_{n\,g}$ is a matrix of size $m \times p$ where m is the number of auxiliary variables in the system and $T_{n\,r}$ is a $m \times p$ matrix. The right hand side is solved by numerically integrating the integrals at each time step. $H_{g\,r}$ is evaluated at the beginning of the simulation. The only derivatives that remain are on the basis function h_r and those can be calculated either analytically in the case of cartesian coordinates or numerically for general geometries. The terms that remain $w_n\left(\tilde{q}, \tilde{v}_{n-1}, ..., \tilde{v}_1\right)$ and $\psi_n\left(\tilde{q}, \tilde{v}_{n-1}, ..., \tilde{v}_1, \mathbf{r}\right)$ are algebraic function of q and v_n which are known (as a result of the basis function expansion of equations (35) and (36)) at all points in space. Gaussian quadrature is performed to approximate the integrals. For a second order method in 1D a 2 point gaussian quadrature is performed. In general in n dimensions a p^n point gaussian quadrature is performed for an order p accurate solution.

The balance laws are solved in a virtually identical manner except a time derivative must also be evaluated, for completeness, start with the balance law multiplied by the basis function set h_r.

$$\int_\Omega \frac{\partial\, \tilde{q}_n}{\partial\, t}\, h_r\, d\Omega + \int_\Omega \nabla \cdot f\left(\tilde{q}, \tilde{v}_1, \tilde{v}_2, ..., \tilde{v}_n\right)\, h_r\, d\Omega = \int_\Omega \psi\left(\tilde{q}, \tilde{v}_n, ..., \tilde{v}_2, \tilde{v}_1, \mathbf{r}\right)\, h_r\, d\Omega\,. \tag{42}$$

move the second term to the right hand side and expand the derivative using integration by parts

$$\int_\Omega \frac{\partial\, \tilde{q}_n}{\partial\, t}\, h_r\, d\Omega = -\int_{\partial\Omega} \left[f\left(\tilde{q}, \tilde{v}_n, ..., \tilde{v}_2, \tilde{v}_1\right)\, h_r\right] \cdot \bar{n}\, d\partial\Omega + \int_\Omega f\left(q, \tilde{v}_n, ..., \tilde{v}_2, \tilde{v}_1\right) \cdot\, \nabla\, h_r\, d\Omega + \int_\Omega \psi\left(\tilde{q}, \tilde{v}_n, ..., \tilde{v}_2, \tilde{v}_1, \mathbf{r}\right)\, h_r\, d\Omega\, = Y_{n\,r} \tag{43}$$

where $Y_{n\,r}$ is the right hand side, i.e., all terms not containing a time derivative. The definition of q is substituted

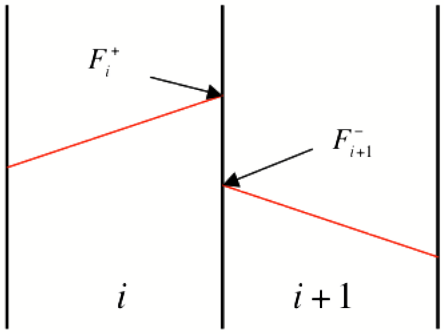

FIG. 1 Figure showing two computational cells separated by vertical lines along with a 2^{nd} order (i.e. piecewise linear) solution in the cell. The flux is calculated as the average of the discontinuous fluxes at the interface plus a dissipation term.

into the first term so that the first term becomes

$$\int_\Omega \frac{\partial \tilde{q}_n}{\partial t}\, h_r \, d\Omega = \sum_{g=0}^{p-1} \frac{\partial \beta_{n\,g}}{\partial t} \int_\Omega h_g \, h_r \, d\Omega = \sum_{g=0}^{p-1} \frac{\partial \beta_{n\,g}}{\partial t}\, H_{g\,r}\,. \tag{44}$$

This gives us equations for the time derivative of $\beta_{n\,g}$ assume $M_{g\,r}$=$H^{-1}_{g\,r}$ then

$$\frac{\partial \beta_{n\,g}}{\partial t} = Y_{n\,r}\, M_{g\,r}. \tag{45}$$

where summation is performed on the repeated index r. Once the right hand side of equation (45) is calculated numerically, the $\beta_{n\,g}$ can be calculated using a second, third or fourth order Runge-Kutta technique. Note that $\beta_{n\,g}$ is a $m \times p$ matrix and so is $Y_{n\,r}$. Notice that the right hand side of equation (43) is identical in form to (38). The right hand side of (43) is therefore calculated in an identical manner.

C. Numerical Fluxes

One important issue in applying discontinuous Galerkin methods is the evaluation of the numerical flux between computational cells. The numerical flux is the term inside the surface integral in equations (43) and (38) namely,

$$F_a = w_n\left(\tilde{q}, \tilde{v}_{n-1}, ..., \tilde{v}_1\right)\, h_r \cdot \bar{n} \tag{46}$$

in the auxiliary equation, and

$$F_c = f\left(\tilde{q}, \tilde{v}_n, ..., \tilde{v}_2, \tilde{v}_1\right)\, h_r \cdot \bar{n} \tag{47}$$

in the conservation equation. Figure 1 illustrates the location where the flux needs to be computed and why the flux is ambiguous. The solution at the interface between cells is discontinuous so the numerical flux calculation depends on averaging in such a way that the scheme remains stable. A simple stable flux, known as the local Lax Friedrichs flux, can be used on the balance variables, in this case

$$\tilde{F}_{i+1/2} = \frac{1}{2}\left[F_i^+ + F_{i+1}^-\right] - \frac{1}{2}|\lambda|\left[q_{i+1}^- - q_i^+\right] \tag{48}$$

λ is chosen to be the largest ideal MHD eigenvalue. In general, for auxiliary variables this same flux can be used, but it needs to be modified by the factor Δt, namely

$$\tilde{F}_{i+1/2} = \frac{1}{2}\left[F_i^+ + F_{i+1}^-\right] - \frac{1}{2}\Delta t|\lambda_a|\left[q_{i+1}^- - q_i^+\right] \tag{49}$$

Choice of fluxes for diffusive systems are discussed in (16) and flux functions for the Schrodinger equation are discussed in (19). We have found that central fluxes ($\lambda_a = 0$ in equation (49)) for the auxiliary variables work well with the 2^{nd} order method, but for 3^{rd} and higher order methods we sometimes choose λ_a in (49) to be the largest ideal MHD eigenvalue.

D. Limiters

For problems with shocks, limiters need to be applied to prevent spurious oscillations at the shocks. In this work limiters are applied either to the balance variables component by component (known as component based limiting) or by applying the limiters to characteristic variables. For component based limiting the formula is quite simple

$$\bar{q}^x = m\left[q^x, q_{i+1}^0 - q_i^0, q_i^0 - q_{i-1}^0\right] \tag{50}$$

where the superscripts represent the particular coefficient of the Legendre polynomial expansion. For a second order scheme a scalar variable q is written as

$$q = q^0 + q^x\left[\frac{x - x_i}{\frac{1}{2}\Delta x}\right] \tag{51}$$

and m is the minmod limiter defined by

$$m\left[a,b,c\right] = \begin{cases} \max\left[a,b,c\right] & \text{if } \text{sign}[a] = \text{sign}[b] = \text{sign}[c] = - \\ \min\left[a,b,c\right] & \text{if } \text{sign}[a] = \text{sign}[b] = \text{sign}[c] = + \\ 0 & \text{otherwise} \end{cases}. \tag{52}$$

Higher order DG methods add additional Legendre polynomials, but standard limiters only look at the first two terms in 1D. Generalization to 2D is accomplished by limiting the coefficient q^y as well. The limiter limits the coefficient q^x of the linear term for each balance variable. The linear coefficient is determined to have been limited if it changes value upon application of the minmod function. In schemes that are 3^{rd} or high order when the linear coefficient is limited all higher order coefficients in the polynomial expansion are set to 0. This is the most basic limiting scheme for n^{th} order DG methods. In general, limiting based on components results in excessive diffusion so a better approach is to limit based on the direction of the non-dispersive waves. In this case the waves could be limited based on a gas dynamic Eigen system or an ideal MHD Eigen system. This paper uses the ideal MHD Eigen system. The balance variables are transformed to characteristic variables using the ideal MHD left eigenvector matrix L. The characteristic variables are written as

$$w^r = L\,q^r\,. \tag{53}$$

Limiting is then performed on the characteristic variables

$$\bar{w}^x = m\left[w^x, w_{i+1}^0 - w_i^0, w_i^0 - w_{i-1}^0\right]\,. \tag{54}$$

Afterwards, the characteristic variables are transformed back to balance variables by multiplying with the right eigenvector matrix R

$$\bar{q}^r = R\,\bar{w}^r\,. \tag{55}$$

The added cost of the characteristic transformation is more than made up for by the gain in accuracy. Note that in this work the electron energy is always limited using component based limiting and none of the auxiliary variables are limited.

Effective limiters are a major focus of research in discontinuous Galerkin methods and a number of more sophisticated limiters have been developed recently including WENO limiters(23; 29), Hermite WENO limiters(1; 20) and high order moment limiters (17). In addition Hesthaven discusses different limiters in his book on discontinuous

Galerkin methods(13). It is suggested that for a production code, to achieve computational benefit of the higher order schemes one or more of these schemes may need to be implemented or perhaps even better schemes developed.

V. RESULTS

A. Convergence

Validation of the order accuracy is performed by calculating the analytic solution to the propagation of a whistler wave in 1 dimension and comparing with solutions computed using the described algorithm. In this case solutions are computed using 2^{nd}, 3^{rd} and 4^{th} order spatial discontinuous Galerkin schemes. Higher order accuracy in the discontinuous Galerkin method is obtained by increasing the number of basis functions, i.e., adding higher order Legendre polynomials, and then increasing the order of quadrature accordingly. The numerical whistler wave solution was obtained by solving the Hall MHD equations with a small perturbation in several field parameters, the exact initial conditions along with the analytic solution are given below

$$e_i = \frac{1}{2}\left(\rho\, U_{i\,y}^2 + \rho\, U_{i\,z}^2\right) + \frac{P_i}{\gamma_i - 1} \tag{56}$$

$$B_z = \left[\frac{B_0\, m_i\, w\, k^2}{q_0\,(B_0^2 k^2 - \rho_0\, w^2\, \mu_0)}\right] \cdot B^{'} \cos\left(k\, x\right) \tag{57}$$

$$\rho\, U_{i\,y} = \left[\frac{B_0}{\mu_0}\frac{k}{w}\right] \cdot B^{'} \sin\left(k\, x\right) \tag{58}$$

$$\rho\, U_{i\,z} = -\left[\frac{m_i\, B_0^2\, k^3}{q_0\, \mu_0\,(\rho_0\, w^2 \mu_0 - B_0^2\, k^2)}\right] \cdot B^{'} \cos\left(k\, x\right) \tag{59}$$

$$B_y = B^{'} \sin\left(k\, x\right) \tag{60}$$

where $k = 8\,\pi$, $B_0 = 0.01$, $q_i = m_i = \mu_0 = n_0 = \rho_0 = 1$, $P_i = P_e = 5 \times 10^{-13}$, $B^{'} = 1 \times 10^{-10}$ and

$$w = \frac{B_0\, k^2\, m_i + B_0\, k\, \left[m_i^2\, k^2 + 4\, m_i\, q_i^2\, n_0 \mu_0\right]^{1/2}}{2\, q_i\, \rho_0\, \mu_0} \tag{61}$$

The numerical solution is solved on the domain $[-0.5, 0.5]$ and evolved until that waves have crossed the domain roughly 2.5 times. Figure 2 shows the error in the computed solution versus the analytic solution for a second, third and fourth order accurate Hall MHD discontinuous Galerkin algorithm. Computed accuracies are calculated and labeled in the caption of figure 3. Results suggest that the computed accuracies match the desired accuracy of the scheme. Figure 2 shows an example solution using only 6 cells across the domain. In these plots the 3^{rd} and 4^{th} order solutions clearly perform much better than the 2^{nd} order solution. In non-linear problems, especially those with shocks, computed accuracies may be substantially below the desired accuracy due to the use of limiters for non-linear stability. The design of effective limiters remains an open issue for this system and discontinuous Galerkin methods in general.

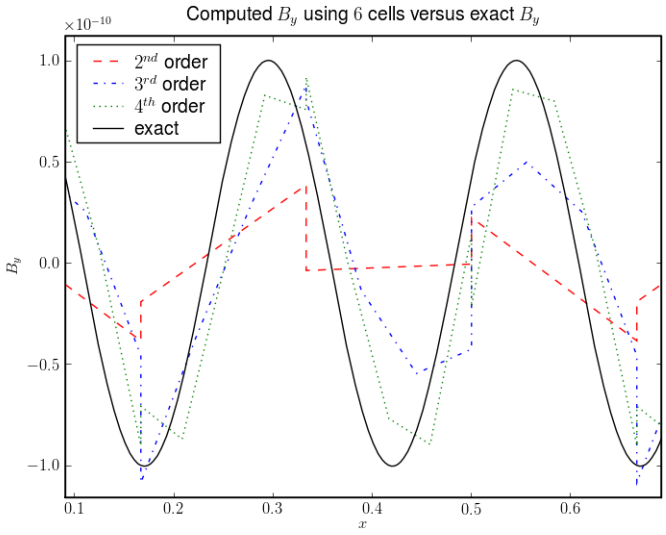

FIG. 2 Plot of B_y after ≈ 2.5 transits using 2^{nd}, 3^{rd} and 4^{th} order solutions. 6 grid cells were used in these simulations so that the differences in the order of accuracy could be observed. Also note that these plots show discontinuities at cell interfaces. Only a subset of the domain is plotted.

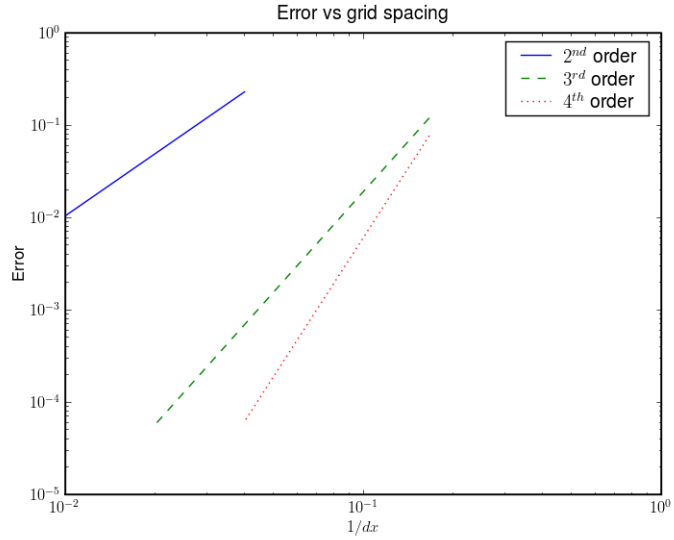

FIG. 3 L_2 norm of the calculated solution vs the analytic solution of B_y normalized by the magntiude of the perturbation. Error is computed after ≈ 2.5 transits of the wave across the domain. Solution shows convergence of 2^{nd}, 3^{rd} and 4^{th} order convergence of the described algorithm for simple 1D whistler wave propagation. Measured order of accuracy (the slope of the lines) shows the second order scheme with order accuracy 2.3, the 3^{rd} order scheme with order accuracy 3.6 and the 4^{th} order scheme with order accuracy 4.9. These results verify the claimed accuracy of the scheme in 1 dimension.

B. Brio and Wu Shock

The Brio and Wu shock problem was recently extended to systems with finite ion inertial length effects in the following works (11; 25) in the framework of the two-fluid plasma system. These same simulations can be run using Hall MHD with diamagnetic drift. The simulations performed in this section use a 2^{nd} order discontinuous Galerkin spatial discretization with 3^{rd} order Runge-Kutta method. The results that follow are Hall MHD solutions to these two-fluid shock problems and will use the same nomenclature. These simulations are mainly presented for validation

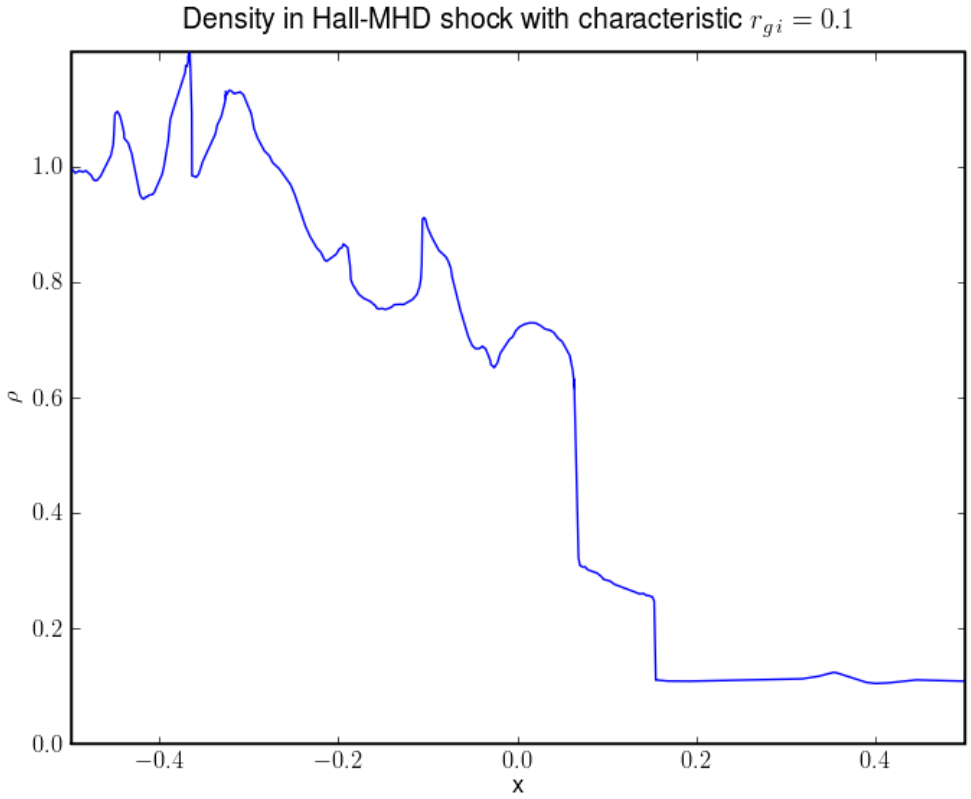

FIG. 4 Hall MHD solution to the Brio and Wu shock problem with characteristic ion Larmor radius of 1/10. The Hall MHD solution agrees quite well with published two-fluid solutions. In this regime the ion demagnetization is extremely important and dispersive non-linear waves dominate the solution.

and illustrate the ability to capture shocks within the Hall MHD framework. The ability to model shocks is particularly important in magneto-inertial fusion concepts such as the FRX-L experiment(27).

Parameters used are $q_i = 10$, $q_e = -10$, and $\epsilon_0 = 1$, $\mu_0 = 1$, $c = 1$, $\gamma_e = \gamma_i = \frac{5}{3}$, $m_i = 1$. The initial conditions are given by $P_e = P_i = 0.5 \times 10^{-4}$, $n_e = n_i = 1.0$ and $B = \left[7.5 \times 10^{-3}, 1.0 \times 10^{-2}, 0\right]$ on the left half of the domain. On the right half of the domain the $P_e = P_i = 0.5 \times 10^{-5}$, $n_e = n_i = 0.125$ and $B = \left[7.5 \times 10^{-3}, -1.0 \times 10^{-2}, 0\right]$ while $U_e = U_i = E = 0$ everywhere.

Figures 4,5 and 6 show the Brio and Wu shock solution with $r_{g\,i} = 1/10$, $r_{g\,i} = 1/100$ and $r_{g\,i} = 1/1000$ respectively where r_{g_1} is the ion Larmor radius calculated using the initial conditions on the left hand side of the shock and normalized by the size of the domain. The ion Larmor radius is calculated as $v_{th\,i}/\omega_{c\,i}$ where $v_{th\,i}$ is the ion thermal velocity and $\omega_{c\,i} = \frac{q_i|B|}{m_i}$. Solutions are quite similar to those calculated previously using the two-fluid equations(11).

These results indicate that much of the physics observed using the full Two-Fluid model can be captured using Hall-MHD in these 1D cases, difference begin appearing at the Debye length scale. However, it should be noted that when the ion inertial length is well resolved the whistler wave is the fastest wave in the Hall MHD solution, in this regime it is often numerically faster to solve the full two-fluid system since the electron inertia adds a whistler wave cutoff resulting in reduced computational requirements for explicit schemes.

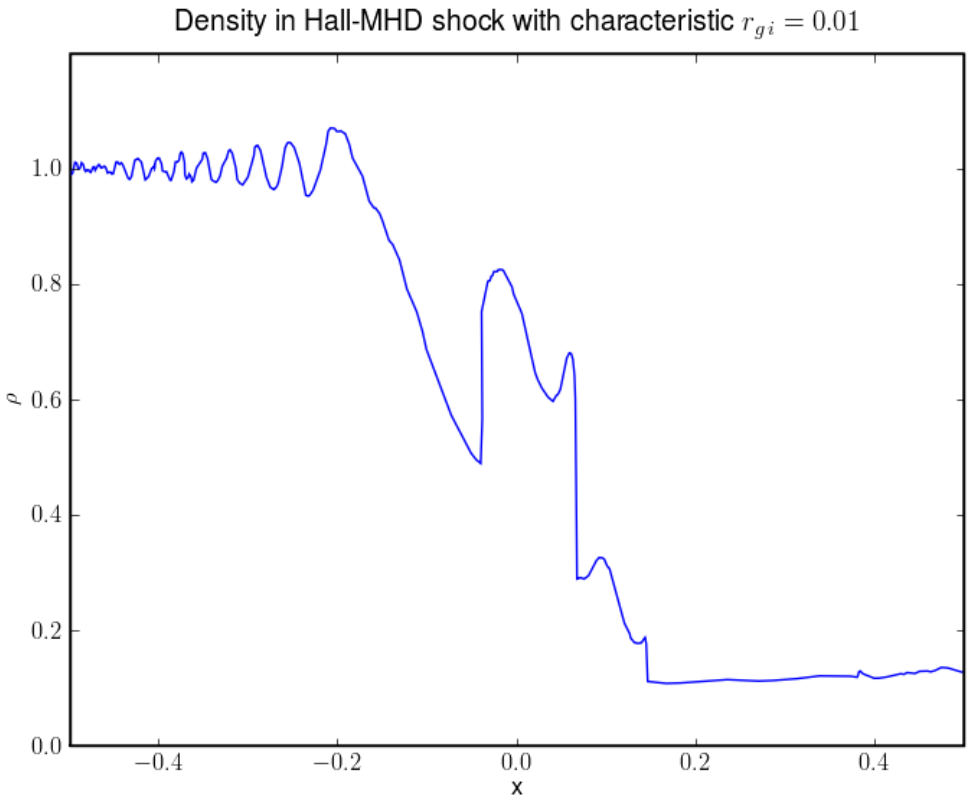

FIG. 5 Hall MHD solution to the Brio and Wu shock problem with characteristic ion Larmor radius of 1/100. Dispersive phenomena dominate on the scale of the ion Larmor radius and lead to the wave trains at the top of the rarefaction.

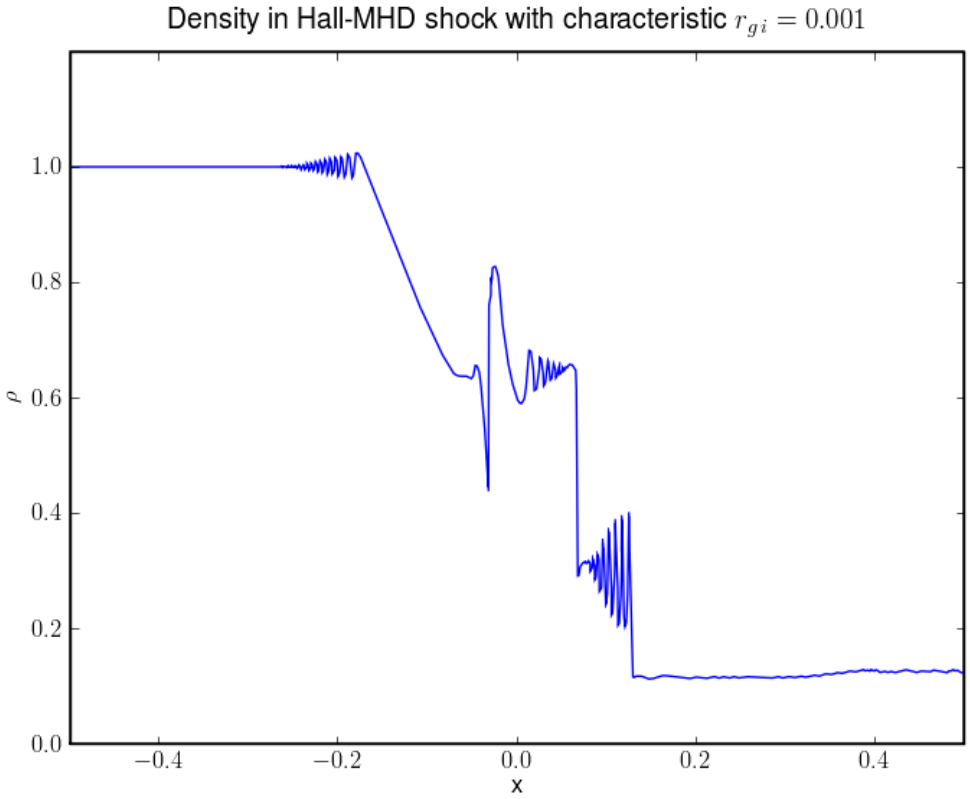

FIG. 6 Hall MHD solution to the Brio and Wu shock problem with characteristic ion Larmor radius 1/1000. Reduction of ion Larmor results in reduced scale where dispersion dominates the solution. Oscillation occur on a much finer scale as a result and the solution looks more MHD-like. Without some sort of collisionality to damp these short wave-length dispersive waves, the system will never actually reproduce the ideal MHD solution. The assumption of high collisionality in ideal MHD is the mechanism that damps the whistler waves.

C. Magnetic Reconnection

Magnetic reconnection is an important test of Hall MHD codes and has become a standard benchmark of codes which include the Hall term. The following results illustrate Hall MHD reconnection using the discontinuous Galerkin approach. A good reference for collisionless reconnection can be found in (3), and in the GEM challenge papers (22; 24).

The GEM challenge magnetic reconnection problem is non-dimensionalized as in (2) where lengths are normalized by the ion inertial length $d = c/\omega_{p\,i} = c\left[\frac{e^2\,n_0}{\epsilon_0\,m_i}\right]^{-\frac{1}{2}}$ time is non-dimensionalized by the ion-cyclotron time $\frac{m_i}{e\,B_0}$ where B_0 is the magnetic field at infinity. The velocities are normalized by the Alfven velocity $V_a = \left[\frac{B_0^2}{\mu_0\,m_i\,n_0}\right]^{\frac{1}{2}}$. Finally current density is non-dimensionalized by $J_0 = \frac{B_0\,w_{p\,i}}{\mu_0\,c}$ and E by $E_0 = V_a\,B_0$. y ranges from $(0, 12.8d)$ and x ranges from $(0, 25.6d)$ and the simulation is run out to $40/\omega_{c\,i}$. Conducting walls are used on the y boundaries and periodic boundaries are used on the x boundaries. In the following $\bar{y} = y - 6.4d$ and $\bar{x} = x - 12.8d$, $\lambda = 0.5\,d$ and the specific heat ratio $\gamma = \frac{5}{3}$. The initial number densities are given by,

$$n = n_0\left[\frac{1}{5} + \operatorname{sech}^2\left(\frac{\bar{y}}{\lambda}\right)\right]. \tag{62}$$

The electron and ion temperatures differ slightly from the GEM challenge problem in that the electron and ion temperatures are equal, this gives the following electron pressure, P_e,

$$P_e = \frac{3}{12\mu_0}B_0^2\,\frac{n_e}{n_0} \tag{63}$$

and ion pressure P_i

$$P_i = \frac{3}{12\mu_0}B_0^2\,\frac{n_i}{n_0}. \tag{64}$$

The electron and ion pressure balance the magnetic field which is given by

$$B_x = B_0\tanh\left(\frac{\bar{y}}{\lambda}\right) + \frac{B_0}{10}\frac{\pi}{L_x}\cos\left(\frac{2\pi\,\bar{x}}{L_x}\right)\sin\left(\frac{\pi\,\bar{y}}{L_y}\right) \tag{65}$$

$$B_y = \frac{B_0}{10}\left[\frac{2\pi}{L_x}\right]\sin\left(\frac{2\pi\,\bar{x}}{L_x}\right)\cos\left(\frac{\pi\,\bar{y}}{L_y}\right) \tag{66}$$

The magnetic field is in equilibrium with with the current J,

$$J_{z\,e} = \frac{\mu_0\,B_0}{\lambda}\operatorname{sech}^2\left(\frac{\bar{x}}{\lambda}\right). \tag{67}$$

However, for the Hall MHD system, J is calculated numerically from B so it is not necessary to set it as an initial condition.

In the GEM challenge papers ion inertia, hyper resistivity or anisotropic pressure terms are frequently sighted as the mechanism which allows the electrons to decouple from the field resulting in reconnection. It's also true however that a scalar pressure can decouple the field from the electron fluid provided that $\nabla\times\frac{\nabla P_e}{n_e\,q_e} \neq 0$, if this condition is not satisfied (such as in the case where pressure depends only on number density and not temperature) then the scalar pressure is not sufficient to decouple the field from the electron fluid. Therefore, in our simulations the decoupling mechanism is the scalar pressure term in the Ohm's law.

Figure 7 shows the reconnected flux versus time for several Hall MHD solutions. Increasing the order of accuracy or grid resolution reduces the amount of numerical dissipation, increasing the reconnected flux vs time towards the correct collisionless result. In these simulation the 2^{nd} order DG spatial discretization is combined with a 3^{rd} order Runge-Kutta discretization. The 4^{th} order solutions show improvement over the second order solution as can be seen by comparison of the 4^{th} order solution on a 64×32 grid with the 2^{nd} order solution on a 128×64 grid. Figure 8 shows plots of mass density for several GEM challenge simulations using the Hall MHD code at time $t = 20/\omega_{c\,i}$ at different grid resolutions and orders of accuracy. Both the 3^{rd} and 4^{th} order solutions show enhanced reconnection

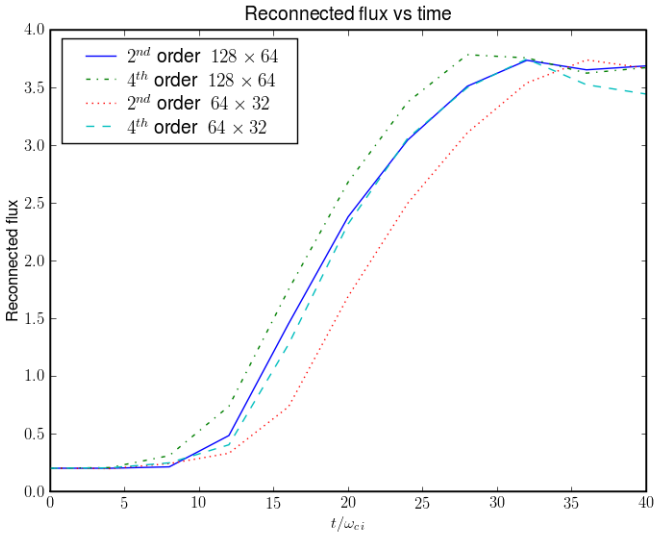

FIG. 7 Plots of reconnected flux calculated using 2^{nd} and 4^{th} order schemes. 3^{rd} order solutions are very similar to the 4^{th} order solution so they are not plotted. The 4^{th} order schemes show improved accuracy over the 2^{nd} order scheme. The reconnected flux for the 4^{th} order solution on a 64×32 grid is very similar to the 2^{nd} order solution on a 128×64 grid indicating that there is some benefit to the higher order accurate methods.

rate over the 2^{nd} order solution for the same grid resolution. Figure 9 shows a vector plot of the in plane magnetic field of the 4^{th} order solution on a 128×64 grid at $t = 25/\omega_{ci}$. The solution clearly shows the reconnected flux and the formation of magnetic islands.

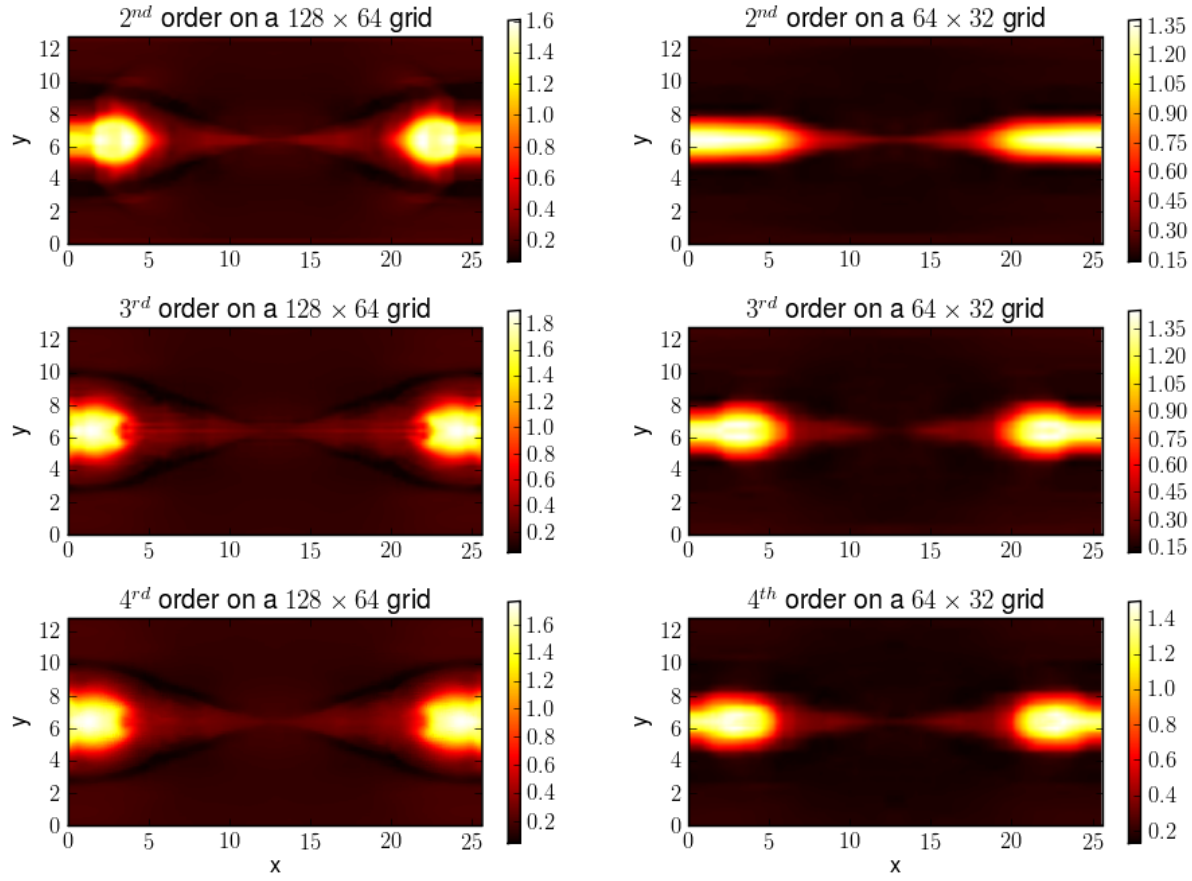

FIG. 8 Density contours for solutions to the magnetic reconnection problem using 2^{nd}, 3^{rd} and 4^{th} order discontinuous Galerkin schemes on 128×64 and 64×32 grids at $t = 20/\omega_{ci}$. Solutions use characteristic based limiters except the 3^{rd} and 4^{th} order solutions on the 128×64 grid where component based limiters are used. The 2^{nd} order solution produces a reduced reconnection as a result of the greater dissipation in the scheme. The 3^{rd} order solution on a 128×64 grid shows striations due to the use of component based limiters, however these striations are not visible in the 4^{th} order 128×64 solution.

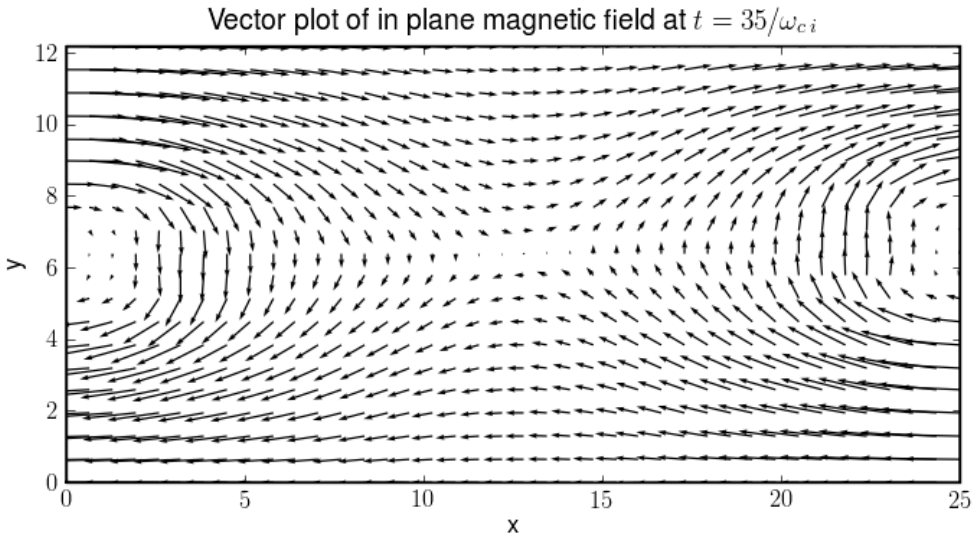

FIG. 9 Vector plot of the magnetic field for the 4th order solution at a resolution of 128×64. Plot shows reconnected field lines as would be expected. Vectors are plotted at $t = 25/\omega_{ci}$

VI. CONCLUSION

A Hall MHD code including diamagnetic drift has been developed using the discontinuous Galerkin method. Results are shown for 2^{nd}, 3^{rd} and 4^{th} order discontinuous Galerkin algorithms. Potential advantages of the discontinuous Galerkin approach are the simplicity with which it can be applied to complex geometries on unstructured grids as well as the straight forward generalization to higher order accuracy. The technique described is explicit and involves a straight forward application of the DG method using auxiliary variables so the large amount of theoretical literature(13) can be applied to the approach. Divergence cleaning is accomplished using the hyperbolic error propagation technique(10) . The simulations of Brio and Wu shock show good agreement with those performed using the full two-fluid model. Simulations of magnetic reconnection agree with prior published results. We observe that the higher order DG approaches have substantial advantage over their lower order counterparts for problems in the linear regime. However, for non-linear problems with shocks (such as magnetic reconnection) the advantages are not as evident due to the use of limiters. Limiters remain an important research topic for discontinuous Galerkin methods, it is key to achieve minimal limiting while preserving non-linear stability and minimizing oscillation in order to observe reduced computational time versus accuracy of n^{th} order methods over 2^{nd} order methods.

References

[1] Dinshaw S. Balsara, Christoph Altmann, Claus-Dieter Munz, and Michael Dumbser. A sub-cell based indicator for troubled zones in rkdg schemes and a novel class of hybrid rkdg+hweno schemes. *Journal of Computational Physics*, 226:586–620, 2007.

[2] J. Birn and et al. Geospace environmental modeling (gem) magnetic reconnection challenge. *Journal of Geophysical Research*, 106(A3):3715–3719, 2001.

[3] D. Biskamp, E. Schwarz, and J.F. Drake. Two-fluid theory of collisionless magnetic reconnection. *Physics of Plasmas*, pages 1002–1009, 1997.

[4] L. Chacon and D.A. Knoll. A 2d high-beta hall mhd implicit nonlinear solver. *Journal of Computational Physics*, 188:573–592, 2003.

[5] Tony F. Chan, Ding Lee, and Longjun Shen. Stable explicit schemes for equations of the schrodinger type. *Siam Journal of Numerical Analysis*, 23(2):274–281, 1986.

[6] Bernardo Cockburn, Suchung Hou, and Chi-Wang Shu. The runge-kutta local projection discontinuous galerkin finite element method for conservation laws iv: Multidimensional case. *Mathematics of Computation*, 54:545–581, 1990.

[7] Bernardo Cockburn, San-Yih Lin, and Chi-Wang Shu. Tvb runge-kutta local projection discontinuous galerkin finite element method for conservation laws iii: One-dimensional systems. *Journal of Computational Physics*, 84:90–113, 1989.

[8] Bernardo Cockburn and Chi-Wang Shu. Tvb runge-kutta local projection discontinuous galerkin finite element method for conservation laws ii: General framework. *Mathematics of Computation*, 52:411–435, 1989.

[9] Bernardo Cockburn and Chi-Wang Shu. The runge-kutta discontinuous galerkin method for conservation laws v: Multidimensional systems. *Journal of Computational Physics*, 141:199–224, 1998.

[10] A. Dedner, F. Kemm, D. Kroner, T. Schnitzer, and M. Wesenberg. Hyperbolic divergence cleaning for the mhd equations. *Journal of Computational Physics*, 175:645–673, 2002.

[11] A. Hakim, J. Loverich, and U. Shumlak. A high resolution wave propagation scheme for ideal two-fluid plasma equations. *Journal of Computational Physics*, 2006.

[12] D.S. Harned and Z. Mikic. Accurate semi-implicit treatment of the hall effect in magnetohydrodynamic computations. *Journal of Computational Physics*, 83:1–15, 1989.

[13] Jan S. Heshaven and Tim Warburton. *Nodal Discontinuous Galerkin Methods, Algorithms, Analysis, and Applications*. Springer, New York, USA, 2008.

[14] Joseph D. Huba. Hall magnetohydrodynamics - a tutorial. In M. Scholer J. Buchner, C.T. Dunn, editor, *Space Plasma Simulation*, pages 166–192. Springer, 2003.

[15] Joseph D. Huba. Numerical methods: Ideal and hall mhd. 2005.

[16] Robert M. Kirby and George Em Karniadakis. Selecting the numerical flux in discontinuous galerkin methods for diffusion problems. *Journal of Scientific Computing*, 22 and 23:2094–2103, June 2005.

[17] Lilia Krivodonova. Limiters for high-order discontinuous galerkin methods. *Journal of Computational Physics*, 226:879–896, 2007.

[18] J. Loverich and U. Shumlak. A discontinuous galerkin method for the full two-fluid plasma model. *Computer Physics Communications*, (169):251–255, 2005.

[19] Tiao Lu, Wei Cai, and Pingwen Zhang. Conservative local discontinuous galerkin methods for time dependent schrodinger equation. *Physics of Plasmas*, 2(1):78–84, 2005.

[20] Hong Luo, Joseph D. Baum, and Rainald Löhner. A hermite weno-based limiter for discontinuous galerkin method on unstructured grids. *J. Comput. Phys.*, 225(1):686–713, 2007.

[21] A. Mangeney, F. Califano, C. Cavazzoni, and P. Travnicek. A numerical scheme for the integration of the vlasov-maxwell system of equations. *Journal of Computational Physics*, 179:495–538, 2002.

[22] A. Otto. Geospace environment modeling (gem) magnetic reconnection challenge: Mhd and hall mhd - constant and current dependent resistivity models. *Journal Of Geophysical Research*, 106:3751–3757, 2001.

[23] Jianxian Qiu. Runge–kutta discontinuous galerkin method using weno limiters. *SIAM J. Sci. Comput.*, 26(3):907–929, 2005.

[24] M. A. Shay, J. F. Drake, B. N. Rogers, and R. E. Denton. Alfvenic collisionless magnetic reconnection and the hall term. *Journal of Geophysical Research*, 106:3759–3772, 2001.

[25] U. Shumlak and J. Loverich. Approximate riemann solver for the two-fluid plasma model. *Journal of Computational Physics*, 187:620–638, 2003.

[26] B. Srinivasan, A. Hakim, and U. Shumlak. A comparison of a high-resolution wave propagation scheme and a runge-kutta discontinuous galerkin scheme for plasma fluid equations. *Under Review in Journal of Computational Physics*.

[27] J. M. Taccetti, T. P. Intrator, G. A. Wurden, S. Y. Zhang, R. Aragonez, P. N. Assmus, C. M. Bass, C. Carey, S. A. deVries, W. J. Fienup, I. Furno, S. C. Hsu, M. P. Kozar, M. C. Langner, J. Liang, R. J. Maqueda, R. A. Martinez, P. G. Sanchez, K. F. Schoenberg, K. J. Scott, R. E. Siemon, E. M. Tejero, E. H. Trask, M. Tuszewski, W. J. Waganaar, C. Grabowski, E. L. Ruden, J. H. Degnan, T. Cavazos, D. G. Gale, and W. Sommars. Frx-l: A field-reversed configuration plasma injector for magnetized target fusion. *Review of Scientific Instruments*, 74(10):4314–4323, 2003.

[28] T. C. Warburton and G. E. Karniadakis. A discontinuous galerkin method for the viscous mhd equations. *Journal of Computational Physics*, 152:608–641, 1999.

[29] Jun Zhu, Jianxian Qiu, Chi-Wang Shu, and Michael Dumbser. Runge-kutta discontinuous galerkin method using weno limiters ii: Unstructured meshes. *J. Comput. Phys.*, 227:4330–4353, 2008.